High-Response, Self-Driving Infrared Photodetection Based on WS_2-Graphene Heterostructure and Metal-Oxide-Semiconductor Field Effect Transistor Structure

Fanxu Wang [1,a]

[1] College of Electronic Information and Optical Engineering, Nankai University,Tianjin, China.

[a] 2252890612@qq.com

Abstract. Two-dimensional materials have garnered increasing attention owing to their exceptional photoelectric properties. Among these materials, WS_2 is characterized by its ability to adjust the band gap by altering the number of material layers and to control its Fermi level through external gate voltage. Graphene exhibits an extensive absorption spectrum ranging from ultraviolet to terahertz waves, alongside high carrier mobility and rapid light response. In this study, we made a photodetector based on WS_2-graphene heterostructure and metal-oxide-semiconductor field effect transistor structure. Leveraging the van der Waals heterojunction formed by these two materials, we aim to amalgamate their respective advantages. Moreover, the Fermi level of the material is modulated via gate voltage manipulation. Subsequently, the sample was tested using a laser with a wavelength of 830 nm. Our research reveal its outstanding photoresponsivity, which holds significant implications for near-infrared band photoelectric detection. This research not only advances the realm of photoelectric detection but also introduces a novel option for near-infrared photoelectric sensing applications.

Keywords: Infrared photoelectric detection; WS_2; Graphene; Heterostructure; Metal-oxide-semiconductor field effect transistor; Imaging.

1. Introduction

1.1 Infrared Photodetector

A photodetector serves as a pivotal optoelectronic device tasked with converting optical signals into electrical ones. [1] Its applications extend across a broad spectrum, encompassing optical fiber communication, industrial automation, biomedical imaging, environmental monitoring, national security defense and various other domains. [2-3] Categorized by the wavelength of absorbed light, photodetectors can be classified into ultraviolet, visible light, infrared, and terahertz detectors. [4] Among these classifications, infrared photodetectors stand out for their capacity to facilitate weather observation, robust anti-interference capabilities, and high-resolution imaging, owing to their ability to capture spontaneous radiation emitted by objects. [5] Consequently, infrared photodetectors find utility in a diverse array of applications, including remote sensing, thermal imaging, biomedical optics, and space communication, among others. [6] Thus, the research and refinement of infrared photodetectors tailored to specific wavelength ranges hold immense significance for advancing these aforementioned fields.

1.2 1.2 Two-dimensional Materials

Based on the principles of the photoelectric effect, the detection wavelength range of a photodetector correlates with the band gap of the semiconductor material employed. The semiconductor materials used in traditional photodetectors are widely used in visible and ultraviolet wavelengths. Examples include GaN-based ultraviolet photodetectors, InGaAs-based short-wave infrared photodetectors, and photodetectors based on Ge and Si for visible light.[7-10] However, as the applications of photodetectors continue to expand, there is a growing demand for enhanced performance, surpassing the capabilities of traditional semiconductor materials. Challenges arise from limitations in controlling material properties, intricate manufacturing processes, and operational temperature constraints. [11-13] Consequently, there is a pressing need to explore alternative

materials and innovative approaches to address these shortcomings and meet evolving application requirements. In recent times, two-dimensional materials have garnered significant attention owing to their remarkable photoelectric properties. [14] Two-dimensional (2D) materials are characterized by intra-layer covalent bonds and interlayer van der Waals interactions. Altering the layer thickness of these materials allows for modulation of the band gap, thereby enabling control over the wavelength range of light absorption. [15] Graphene exhibits an exceptionally broad absorption spectrum spanning from ultraviolet to terahertz waves, along with high carrier mobility and rapid light response. Nevertheless, its intrinsic gapless band structure results in low light absorption for single-layer graphene. Additionally, the fast recombination rate of graphene carriers contributes to diminished photoresponsivity in photodetectors constructed with graphene. As such, while the properties of graphene render it promising for various applications, including photodetection, its limitations necessitate further exploration and refinement in order to optimize its performance in photonic devices. [16-17] Black phosphorus possesses the feature of an adjustable band gap, which varies with its thickness, rendering it responsive across a broad spectrum ranging from ultraviolet to near-infrared light regions. Furthermore, black phosphorus demonstrates high carrier mobility, contributing to its favorable electrical and optical response characteristics. However, black phosphorus is poor in stability and needs to be treated carefully to resist the erosion of oxygen and water. [18-20] Topological materials also have garnered attention in the realm of photoelectric detection in recent years. Topological insulators generally show a metallic state with an insulating phase and zero band gap at the boundary or surface. At the boundary or surface of the material, Dirac-type electrons are present. Consequently, collision scattering between electrons is mitigated, thereby minimizing power loss. [21-22] Due to the above characteristics, the device made of topological insulator has the characteristics of high speed and low energy consumption and the photodetector made of it has a wide detection range. [23] However, due to its structural characteristics, topological materials cannot be separated into very thin layers. As a consequence, detectors constructed from topological materials frequently manifest a high dark current, thereby posing constraints on enhancing photoresponsivity. The transition metal sulfide also has the characteristics that the band gap can be adjusted by changing the number of material layers and its Fermi level can be controlled by external gate voltage. [24-25] This feature holds significant significance for the infrared band detection, an area highly demanded within the industry.

1.3 Summarization of This Work

In the pursuit of optimal photoelectric detection, the selection of appropriate 2D semiconductor materials with high carrier mobility and favorable light absorption properties is paramount, considering the unique attributes inherent to different 2D materials. In this work, geared towards infrared band detection, we initially fabricated an Au-WS2-Au structure detector, enhancing its optical response through incremental bias voltage adjustments. Building upon this foundation, we developed a photodetector predicated on a WS2-graphene heterostructure, implementing a method to modulate the Fermi level of WS2 via gate voltage application. It is found that the detector has good photoelectric response characteristics.

2. Results and Discussion

2.1 Material Characterization and Device Preparation

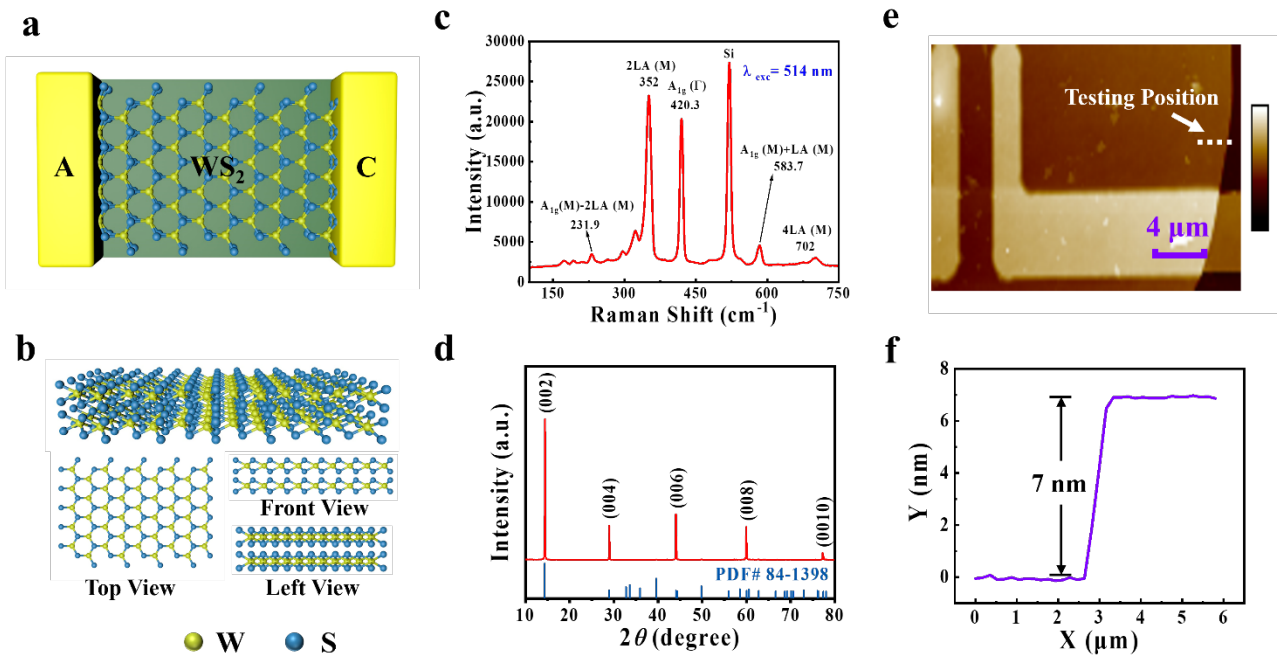

Figure 1. Material characterization of the Au-WS2-Au structure photodetector sample. (a) Schematic diagram of device structure simulation. (b) Overall molecular structure of WS2 and top view, front view, left view. (c) Raman spectra of the sample. (d) X-ray diffraction pattern of the sample. (e) AFM image of the sample, with white dotted line for test location and purple solid line for legend. (f) Thickness data diagram of the sample.

The tungsten disulfide sheet was transferred to the substrate with gold-plated electrode by the all-dry transfer method. The top view of the device is shown in Figure 1a. Tungsten disulfide is a typical two-dimensional material with a close-packed hexagonal crystalline layered structure. One tungsten atom and six sulfur atoms are bonded through covalent bonds, and a metallic tungsten atom layer is sandwiched by two sulfur atom layers. [26] The schematic diagram of its molecular structure is shown in Figure 1b. Figure 1c shows the Raman spectrum of the sample. It can be observed that there are obvious characteristic peaks at 352 cm-1, 420.3 cm-1 and 520 cm-1. Figure 1d shows the X-ray diffraction pattern of the sample, with obvious peaks at 14.44°, 28.98°, 44.04°, 59.93° and 77.23°, corresponding to the (002), (004), (006), (008) and (0010) planes of the sample respectively. Figures 1c and 1d confirm the validity of the material constituting the sample through measurement data, similar to those previously reported. [27-28] The atomic force microscope (AFM) image of the sample is depicted in Figure 1e, with corresponding data presented in Figure 1f. Upon examination of the data image, it is evident that the thickness of tungsten disulfide in the sample measures approximately 7 nm. The pertinent data presented in Figure 1 validate the efficacy of the sample device preparation and characterize the thickness of the device, thereby ensuring the precision of subsequent experiments.

2.2 Photoelectric Properties of Au-WS2-Au Structure

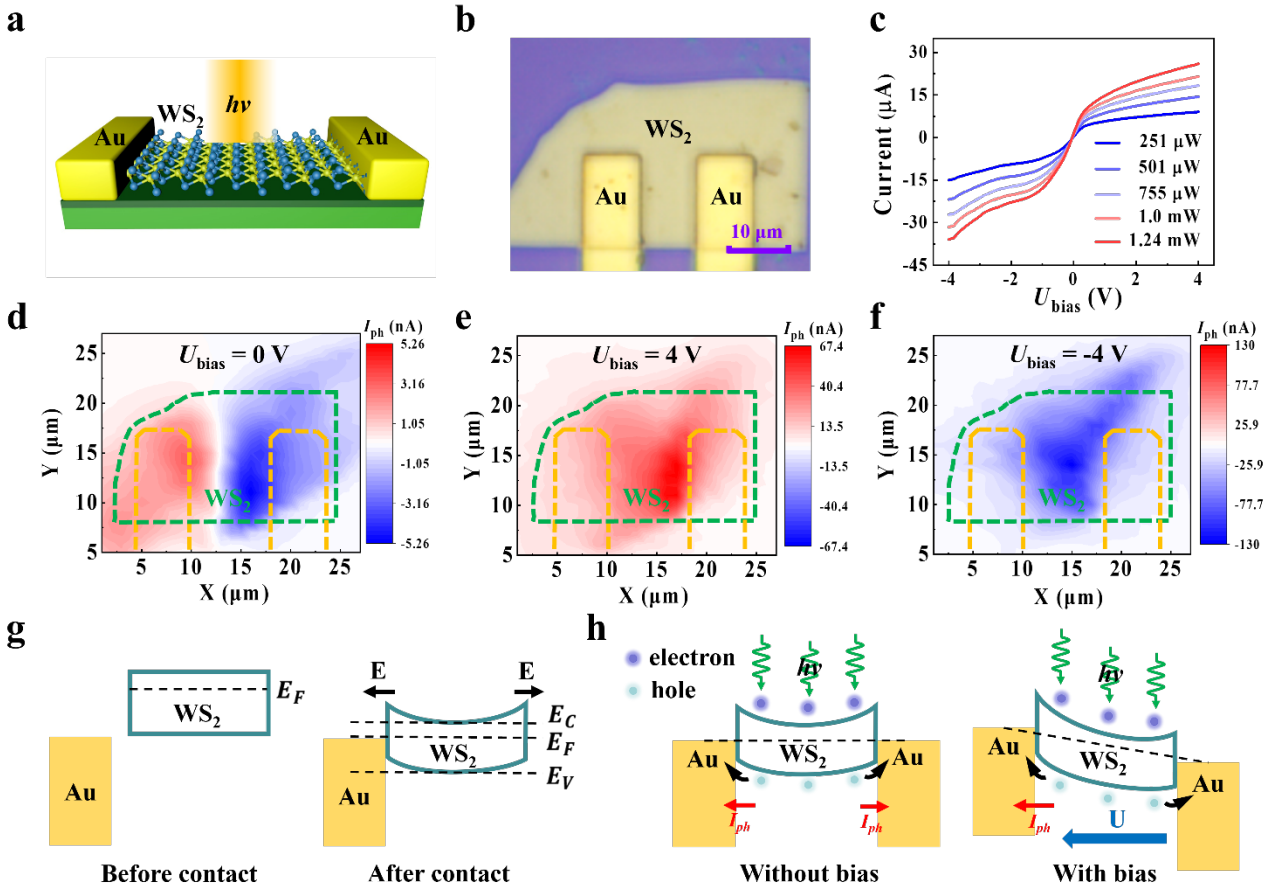

Figure 2. The device structure of the Au-WS2-Au structure photodetector sample and the photoresponsivity at different bias. (a) Device structure of the photodetector based on Au-WS2-Au structure. (b) The optical image of the photodetector based on Au-WS2-Au structure. (c) Current-voltage characteristic curve of the device with different incident power. (d) - (f) Photocurrent mapping of the device under 830 nm laser illumination at Ubias of 0 V, 4 V, and -4 V. (g) The energy band diagram before and after WS2 contacts with Au. E is the built-in electric field, EC is the conduction band, EF is the Fermi level, and EV is the valence band. (h) The energy band diagrams of Au-WS2-Au structure with and without bias in the presence of light.

Figure 2 shows the data diagram of the Au-WS2-Au structure photodetector (PD). This sample enhances the photoresponsivity by changing the voltage at both ends of the PD. Figure 2a is the schematic diagram of the device structure. Figure 2b is the optical image of the PD. For the purpose of photoelectric detection in the near infrared band in this study, light with a wavelength of 830 nm was used for imaging. Figure 2c shows the output current characteristic curve measured under varying incident power levels. It is evident that the photocurrent increases with the rise in power at the same bias voltage, indicating the favorable optical response characteristics of the device. Under the condition of increasing the bias voltage at both ends, the photocurrent of the PD increases significantly. Within a certain range, the photocurrent increases proportionally with the rise in bias voltage. Given that both sides of the device exhibit identical Schottky barriers generated by metal-semiconductor contact, the resulting photocurrent displays symmetry concerning positive and negative bias, as depicted in the output current curve. Figure 2d, 2e and 2f are the photocurrent mapping of the device at different bias voltage. Under the test conditions illustrated in the figure, a comparison of the scanning photocurrent at Ubias values of 0 V, 4 V, and -4 V reveals that at 0 V, the current ranges from -5 nA to 5 nA, while at ±4 V, it varies from -100 nA to 100 nA. This analysis indicates a

significant increase in the photocurrent of the PD under both positive and negative bias voltage conditions. Figure 2g elucidates the mechanism behind the enhancement of photocurrent through an energy band diagram. In the absence of bias, photogenerated carriers cross the same Schottky barrier on both sides and diffuse from the semiconductor material to the metal electrode on both sides, resulting in a low photocurrent. However, under external bias conditions, photogenerated charge carriers move under the action of electric field. And because of the effect of external electric field, the energy band of metal and semiconductor materials changes, thereby augmenting the movement of charge carriers and consequently enhancing the photoresponsivity.

2.3 Photoelectric Properties of Metal-oxide-semiconductor Field Effect Transistor

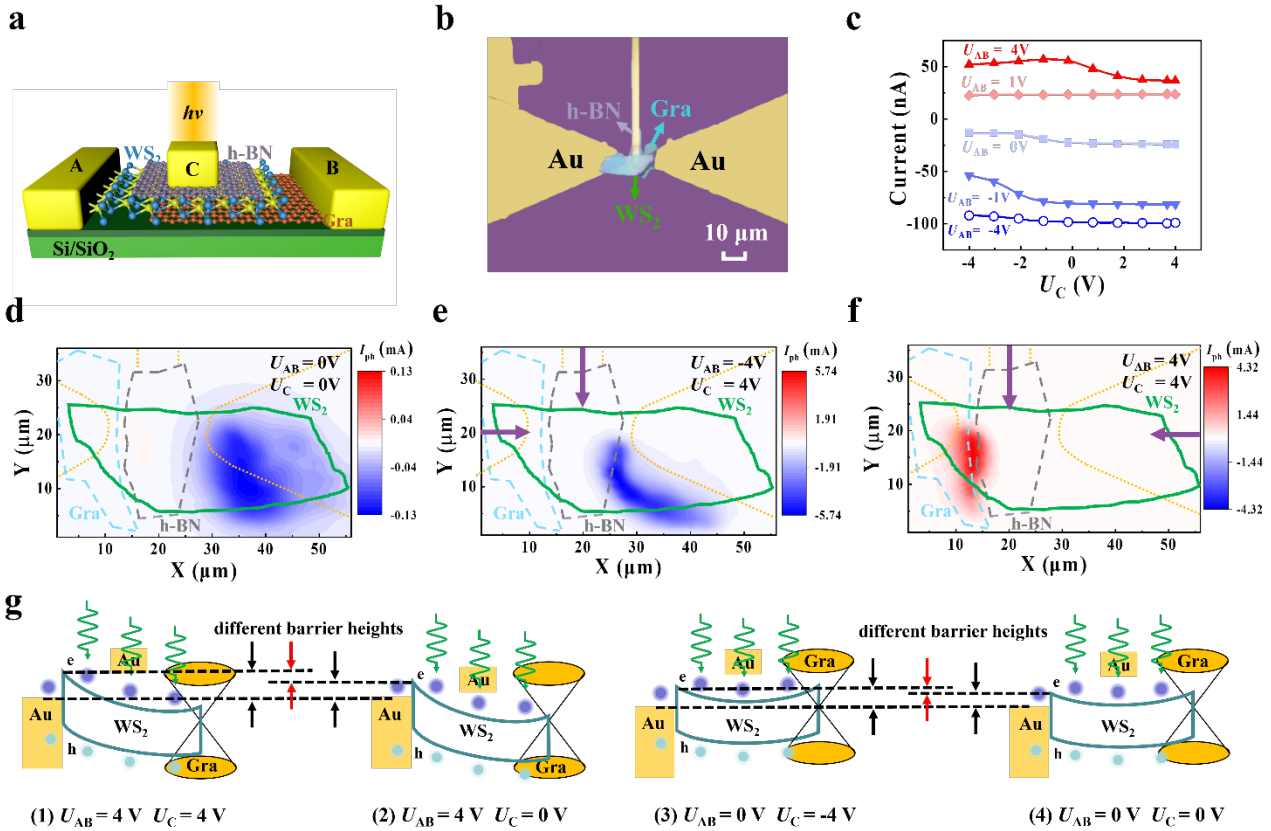

Figure 3. The device structure of photodetection based on WS2-graphene heterostructure and metal-oxide-semiconductor field effect transistor and the photoresponsivity at different bias voltage. (a) Schematic diagram of device structure. (b) The optical image of the photodetector, white solid lines for the legend. (c) The transfer characteristic curve of the device describes the relationship between the output current and gate voltage under UAB conditions of -4 V, -1 V, 0 V, 1 V, and 4 V respectively. (d) - (f) Photocurrent mapping of the device under 830 nm laser illumination at UAB = 0 V UC = 0 V, UAB = -4 V UC = 4 V and UAB = 4 V UC = 4 V respectively. (g) Energy band diagrams of Au-WS2-Graphene structure, (1) and (2) are the energy band diagrams at different UC when UAB is 4V; (3) and (4) are the energy band diagrams at different UC when UAB is 0V.

A heterojunction emerges when two distinct materials make contact. Two-dimensional layered materials have the capacity to create van der Waals heterojunctions through interlayer van der Waals interactions. The contact between tungsten disulfide and graphene to form a van der Waals heterojunction amalgamates the advantages inherent in both materials. This combination enhances the light absorption rate of the device and results in a high light response speed, surpassing the performance of individual materials. [29-30] In addition, it is found that the gate voltage can regulate the Fermi level of two-dimensional materials. [31] Hexagonal boron nitride (h-BN) is a good material to make insulation for metal-oxide-semiconductor field effect transistor. It has an atomic level of flat

surface, high carrier mobility and a lattice mismatch of less than 1.7 % with graphene. [32] It's a good choice for our work. On the basis of Figure 2, we also use all-dry transfer method to transfer a graphene sheet onto the substrate, thereby creating a WS2-graphene heterojunction. Differing from Figure 2, we introduced an h-BN layer onto the heterojunction to serve as the insulation layer for the gate. Subsequently, gold-plated electrodes were deposited onto the h-BN insulation layer as the gate, thus forming a field-effect transistor structure. Figure 3a is the schematic diagram of the device structure of the sample. Figure 3b is the optical image of the PD. Figure 3c shows the transfer characteristic curve of the device. It is evident from the curve depicted in the figure that applying a bias voltage between the drain and source leads to an enhancement in the current of the device. Different from Figure 2, due to the Schottky barrier generated by metal-semiconductor contact on both sides of the device and the van der Waals heterojunction formed by the combination of two different semiconductor materials, the work function difference of several materials is different, resulting in different barrier heights on both sides. When UAB is 4 V, the current is about 50 nA. When UAB is -4 V, the current is about -100 nA. It can also be observed in the figure that when the gate voltage UC changes, the photocurrent response changes, reflecting the gate-voltage regulation characteristics of the device and the regulation effect is different under different UAB conditions. Figure 3d shows the photocurrent mapping of the device without gate voltage and drain-source voltage. The presence of photocurrent confirms the self-driving characteristic of the device. This disparity arises from the difference in barrier height on both sides, resulting in varying sizes of the current formed by the photogenerated carrier drifting to each side under unbiased voltage conditions, ultimately resulting in a short circuit current. Figure 3e and Figure 3f show the photocurrent mapping of the device under the conditions of gate voltage and drain-source voltage. A significant photocurrent can be found in the range of ±5 mA. It proves that the photoresponsivity is significantly enhanced under the influence of heterojunction formation and gate voltage regulation. Figure 3g analyzes the effect of gate voltage regulation by using energy band diagram. Since the work function of tungsten disulfide is lower than that of Au and graphene, the energy bands on both sides are bent upward. Under the influence of applied gate voltage, the Fermi level of tungsten disulfide decreases, leading to a reduction in the Fermi energy level difference between WS2, Au, and graphene on both sides. Consequently, this decrease results in a reduction in the barrier height after contact. Therefore, the photogenerated charge carriers are easier to drift under the action of electric field, resulting in a more obvious photocurrent. The comparison between (1) ~ (2) and (3) ~ (4) reveals that the variation in barrier height at UAB = 4 V is more pronounced compared to that at UAB = 0 V. This observation highlights the disparity in gate-controlled effects under different UAB conditions.

2.4 Application of Our Photodetector

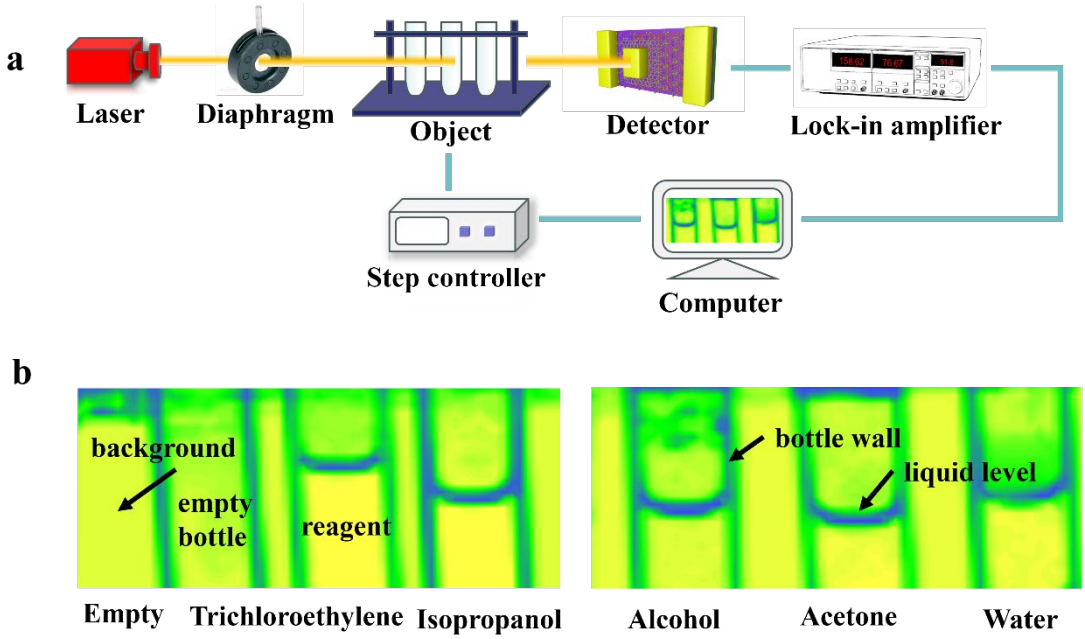

Figure 4. Schematic diagram of the imaging application of WS2-Graphene heterojunction photodetectors. (a) Schematic diagram of the imaging system. (b) Imaging results.

To further demonstrate the detection performance of the sample, it undergoes testing for the photodetector imaging application, as illustrated in Figure 4. Utilizing a comprehensive imaging system, as depicted in Figure 4a, the samples selected for testing comprise empty bottles and reagent bottles containing trichloroethylene, isopropyl alcohol, alcohol, acetone, and water. The detectable light traverses through the diaphragm and illuminates the sample under measurement, subsequently being captured by a PD for imaging. The high-precision stepper motor, controlled by the computer, precisely moves the sample to be measured both horizontally and vertically. This motion enables the detector to receive light signals from various positions. Upon conversion of the optical signal into an electrical one, it is transmitted to a computer via a phase-locked amplifier. Subsequently, the computer conducts imaging based on the acquired data size. Following color processing, the resultant data graph is depicted in Figure 4b. Prominent sample structures, including reagents, bottle walls, and liquid levels, are clearly discernible, proving the excellent photoelectric detection performance of the sample within the near-infrared band.

3. Conclusions

In conclusion, we initially fabricated an Au-WS2-Au structure PD and observed an enhancement in photoresponsivity with increased bias voltage. Building upon this finding, we utilized a WS2-graphene heterostructure to construct a metal-oxide-semiconductor field-effect transistor, which exhibited favorable light response characteristics. Subsequently, we conducted application tests, wherein the test result images effectively distinguished various test objects, reaffirming the outstanding detection performance of our PD. Furthermore, our study utilized a laser wavelength of 830 nm for testing, showcasing the robust performance of our PD in the near-infrared band and its promising potential in the realm of infrared photoelectric detection.

Acknowledgements

Thank you to the Shanghai Institute of Technical Physics for their support in this work.

References

[1] Wang F, Zou X, Xu M, et al. (2021). “Recent progress on electrical and optical manipulations of perovskite photodetectors, ” Advanced Science (2021), 8(14): 2100569.
[2] Su L, Yang W, Cai J, et al. (2017). “Self‐powered ultraviolet photodetectors driven by built‐in electric field, ” Small (2017), 13(45): 1701687.
[3] Dong Z, Yu W, Zhang L, et al. (2021). “Highly efficient, ultrabroad PdSe2 phototransistors from visible to terahertz driven by mutiphysical mechanism, ” ACS nano (2021), 15(12): 20403-20413.
[4] Chen H, Liu H, Zhang Z, et al. (2016). “Nanostructured photodetectors: from ultraviolet to terahertz, ” Advanced Materials (2016), 28(3): 403-433.
[5] Zha J, Luo M, Ye M, et al. (2022). “Infrared photodetectors based on 2D materials and nanophotonics, ” Advanced Functional Materials (2022), 32(15): 2111970.
[6] Dai M, Wang C, Ye M, et al. (2022). “High-performance, polarization-sensitive, long-wave infrared photodetection via photothermoelectric effect with asymmetric van der Waals contacts, ” ACS nano (2022), 16(1): 295-305.
[7] Butun B, Tut T, Ulker E, et al. (2008). “High-performance visible-blind GaN-based pin photodetectors, ” Applied Physics Letters (2008), 92(3).
[8] Yang Y, Wang W, Zheng Y, et al. (2021). “Defect effect on the performance of nonpolar GaN-based ultraviolet photodetectors, ” Applied Physics Letters (2021), 118(5).
[9] Rezaei M, Park M S, Rabinowitz C, et al. (2019). “InGaAs based heterojunction phototransistors: Viable solution for high-speed and low-noise short wave infrared imaging, ” Applied Physics Letters (2019), 114(16).
[10] Yanikgonul S, Leong V, Ong J R, et al. (2021). “Integrated avalanche photodetectors for visible light, ” Nature communications (2021), 12(1): 1834.
[11] Fang J, Zhou Z, Xiao M, et al. (2020). “Recent advances in low‐dimensional semiconductor nanomaterials and their applications in high‐performance photodetectors, ” InfoMat (2020), 2(2): 291-317.
[12] Michel J, Liu J, Kimerling L C. (2010). “High-performance Ge-on-Si photodetectors, ” Nature photonics (2010), 4(8): 527-534.
[13] Long M, Wang P, Fang H, et al. (2019). “Progress, challenges, and opportunities for 2D material based photodetectors, ” Advanced Functional Materials (2019), 29(19): 1803807.
[14] Konstantatos G. (2018). “Current status and technological prospect of photodetectors based on two-dimensional materials, ” Nature communications (2018), 9(1): 5266.
[15] Rao G, Wang X, Wang Y, et al. (2019). “Two‐dimensional heterostructure promoted infrared photodetection devices, ” InfoMat (2019), 1(3): 272-288.
[16] Koppens F H L, Mueller T, Avouris P, et al. (2014). “Photodetectors based on graphene, other two-dimensional materials and hybrid systems, ” Nature nanotechnology (2014), 9(10): 780-793.
[17] Guan X, Yu X, Periyanagounder D, et al. (2021). “Recent progress in short‐to long‐wave infrared photodetection using 2D materials and heterostructures, ” Advanced Optical Materials (2021), 9(4): 2001708.
[18] Chen X, Lu X, Deng B, et al. (2017). “Widely tunable black phosphorus mid-infrared photodetector, ” Nature communications (2017), 8(1): 1672.
[19] Das S, Zhang W, Demarteau M, et al. (2014). “Tunable transport gap in phosphorene, ” Nano letters (2014), 14(10): 5733-5739.
[20] Xing C, Zhang J, Jing J, et al. (2019). “Preparations, properties and applications of low-dimensional black phosphorus, ” Chemical Engineering Journal (2019), 370: 120-135.
[21] Hasan M Z, Kane C L. (2010). “Colloquium: topological insulators, ” Reviews of modern physics (2010), 82(4): 3045.
[22] Wang B, Zhong S, Xu P, et al. (2020). “Recent development and advances in Photodetectors based on two-dimensional topological insulators, ” Journal of Materials Chemistry C (2020), 8(44): 15526-15574.
[23] Zhang H, Zhang X, Liu C, et al. (2016). “High-responsivity, high-detectivity, ultrafast topological insulator Bi2Se3/silicon heterostructure broadband photodetectors, ” ACS nano (2016), 10(5): 5113-5122.
[24] Heine T. (2015). “Transition metal chalcogenides: ultrathin inorganic materials with tunable electronic properties, ” Accounts of chemical research (2015), 48(1): 65-72.
[25] Jariwala D, Sangwan V K, Lauhon L J, et al. (2014). “Emerging device applications for semiconducting

two-dimensional transition metal dichalcogenides, ” ACS nano (2014), 8(2): 1102-1120.
[26] Schutte W J, De Boer J L, Jellinek F. (1987). “Crystal structures of tungsten disulfide and diselenide, ” Journal of Solid State Chemistry (1987), 70(2): 207-209.
[27] Lee C, Kim S T, Jeong B G, et al. (2017). “Tip-enhanced Raman scattering imaging of two-dimensional tungsten disulfide with optimized tip fabrication process, ” Scientific reports (2017), 7(1): 40810.
[28] Selvi E, Ma Y, Aksoy R, et al. (2006). “High pressure X-ray diffraction study of tungsten disulfide, ” Journal of physics and chemistry of solids (2006), 67(9-10): 2183-2186.
[29] Chen J, Ouyang W, Yang W, et al. (2020). “Recent progress of heterojunction ultraviolet photodetectors: materials, integrations, and applications, ” Advanced Functional Materials (2020), 30(16): 1909909.
[30] Rao G, Wang X, Wang Y, et al. (2019). “Two‐dimensional heterostructure promoted infrared photodetection devices, ” InfoMat (2019), 1(3): 272-288.
[31] Zhao Y, Xu K, Pan F, et al. (2017). “Doping, contact and interface engineering of two‐dimensional layered transition metal dichalcogenides transistors, ” Advanced Functional Materials (2017), 27(19): 1603484.
[32] Wang J, Ma F, Liang W, et al. (2017). “Electrical properties and applications of graphene, hexagonal boron nitride (h-BN), and graphene/h-BN heterostructures, ” Materials Today Physics (2017), 2: 6-34.